Nuclear Engineering and Design 328 (2018) 321–332

Contents lists available at ScienceDirect

Nuclear Engineering and Design

journal homepage: www.elsevier.com/locate/nucengdes

A CFD analysis of the flow dynamics of a directly-operated safety relief valve

N.L. Scuro[a,*], E. Angelo[b], G. Angelo[a,c], D.A. Andrade[a]

[a] Instituto de Pesquisas Energéticas e Nucleares, Avenida Lineu Prestes, 2242, Centro de Engenharia Nuclear, 05508-000 São Paulo, SP, Brazil
[b] Universidade Presbiteriana Mackenzie, Rua da Consolação, 930, 01302-907 São Paulo, SP, Brazil
[c] Centro Universitário FEI, Avenida Humberto de Alencar Castelo Branco, 3972-B, 09850-901 São Bernardo do Campo, SP, Brazil

ABSTRACT

A three-dimensional numerical study on steady state was designed for a safety relief valve using several openings and inlet pressures. The ANSYS-CFX® commercial code was used as a CFD tool to obtain several properties using dry saturated steam revised by IAPWS-IF97. Mass flow and discharge coefficient calculated from simulations are compared to the ASME 2011a Section 1 standard. The model presented constant behavior for opening lifts smaller than 12 mm and is very reasonable when compared to the standard (ASME). In addition, the conventional procedure to design normal disc force assumes that all the fluid mechanical energy was converted into work; however, the CFD simulations showed that average normal disc force is about 19% lower than theoretical ASME force, which could prevent the valve oversizing. A numerical validation was conducted for a transonic air flow through a converging–diverging diffuser geometry to verify the solver's ability to capture the position and intensity of a shockwave: the results showed good agreement with the benchmark experiments.

1. Introduction

PWR nuclear power plants contain a primary pressurized circuit of water at liquid state, which is responsible for heating a secondary steam generator system. Both systems must have their flow, pressure, temperature and other physical properties controlled. Under overheating events, the increasing pressure inside the vessel can lead to an accident if it is not controlled to be within the project limit range. Safety relief valves installed at each circuit can reduce internal pressure by discharging water (Jan, 1980). Several factors determine the stability of the safety relief valves in order to guarantee their behavior for nuclear or industrial use (Darby, 2013). However, six main factors are listed below:

(i) Valve design, Kasai (1968);
(ii) Spring pre-deformation (x), Bazsó & Hös (2013);
(iii) Length of the inlet pipeline (L), Thomann (1976);
(iv) Valve opening length (lift) (δ), Song et al. (2014);
(v) Regulator rings position (x′), Green & Woods (1973);
(vi) Pressure vessel volume (ϑ), Song et al. (2014).

These factors have been studied, many times, analyzing the influence of one factor, because, due to the large number of variables, a complete analysis is generally not viable. Thus, some studies are presented to explain the influence of each factor on the valve stability.

Vu et al. (1994) performed a three-dimensional numerical study of a safety relief valve working with oxygen gas, aiming to better understand the appearance of erosion zones. This study showed that the flow created multiple vortices, which induced a chaotic cycle and oscillatory behavior. This situation caused a vibrational movement that caused many impacts to the nozzle, breaking and bringing the circuit to danger; therefore, the valve design influenced the chaotic behavior of the valve. In addition, Vu et al. (1994) showed that the lack of maintenance at a safety relief valve originated little solid waste deposits in the nozzle, increasing its internal friction force. The generation of heat in the throat area increased with the intensive use of the valve, resulting in little sparks. Due to the fluid used, small regions initiated the combustion process, eroding many parts of the valve. This behavior was posteriorly discovered as a function of disc chattering.

In order to study the influence of pressure distribution inside the relief valve, Francis & Betts (1998) conducted a similar study to the one proposed by Vu et al. (1994). The researchers have observed the existence of a critical backpressure condition of work that leads to unstable behavior, but due the number of instability factors, such behavior cannot be immediately simplified.

Among the instability factors, spring pre-deformation was noticed as one of the most delicate factors to instability (MacLeod, 1985). As observed in their study, the more the spring is deformed, the more difficult it becomes to open it for the same designed pressure. Therefore, with the increase in spring pre-deformation, higher inlet pressure is

* Corresponding author.
E-mail addresses: nikolas.scuro@ipen.br (N.L. Scuro), eangelo@mackenzie.br (E. Angelo), gangelo@fei.edu.br (G. Angelo), delvonei@ipen.br (D.A. Andrade).

https://doi.org/10.1016/j.nucengdes.2018.01.024
Received 3 May 2017; Received in revised form 8 January 2018; Accepted 9 January 2018
Available online 20 January 2018
0029-5493/ © 2018 Elsevier B.V. All rights reserved.

Nomenclature

A	area (m^2)
a	disc lift (m)
d	diameter (m)
h	specific enthalpy (J/kg)
k	turbulent kinetic energy (m^2/s^2)
k_d	discharge coefficient [1]
$\dot{m}$	mass flow rate (kg/s)
p	pressure (Pa)
P_k	shear turbulent production ($kg/m.s^2$)
Pr_t	turbulent Prandtl number [1]
$\overline{U_i}$	vector of velocity (m/s)
$\overline{u_i' u_j'}$	Reynolds stress (m^2/s^2)
λ	thermal conductivity (W/m.K)
ε	turbulence dissipation rate (m^2/s^3)
μ	dynamic viscosity (Pa.s)
ρ	density (kg/m^3)
τ	shear stress (Pa)

Superscripts

–	average value
′	fluctuation component

Subscripts

eff	effective
IN	inlet
N	nozzle
OUT	outlet
R	real
S	standards
t	turbulent
T	throat
tot	total

k−ε (constants)

C_μ	0.09
$C_{\varepsilon 1}$	1.44
$C_{\varepsilon 2}$	1.92
σ_k	1.00
σ_ε	1.30

necessary to the opening of the valve, increasing the chance of generating a shockwave.

Another factor related to valve instability is how the inlet pressure is increasing. In other words, if the inlet pressure increases slowly with a constant rate, the mass spring system would have a large time interval to align with natural frequencies, which should be avoided. Otherwise, the valve would be subjected to a longer vibrational period, that could cause severe impacts between the nozzle and the disc (Hayashi et al., 1997; Hös et al., 2014). Therefore, when the inlet pressure on safety relief valve inlet has small oscillations, it can be controlled with spring pre-deformation, thus reducing vibration on the disc (Botros et al., 1997; Chabane et al., 2009; Misra et al., 2002). Nevertheless, the more the fluctuation of the developed flow leads the valve to its natural frequency, the greater will be the fluctuations inside the valve, (Funk, 1964; Botros et al., 1997).

Nevertheless, valve design and components are not the only factors that can lead to instability. A theoretical research proposed by Thomann (1976) indicates the existence of a link between the length of the inlet pipe and valve static equilibrium. According to Kasai (1968), an oscillatory behavior could be aggravated or delayed by the length of the inlet pipe. This pipe length would be theoretically responsible for eliminating fluctuations of inlet pressure, thus eliminating abrupt changes in the velocity field and pressure.

Green and Woods (1973) conducted a study related not just to geometric factor, but also to flow properties. The nonlinear behavior of the valve could be caused by four factors: (i) laminar flow transition to turbulent during the valve process of opening and closing, (ii) balance restoring force, (iii) hysteresis and (iv) fluctuation of the downstream pressure. The same researcher verified the existence of a relation between the regulator rings position and the force transmitted to the valve disc, influencing in the stability.

Another alternative to analyze the influence of many factors in safety relief valves is their physical/mathematical analysis, by using specific numerical codes. Lee et al. (1982) showed the influence of a safety relieve valve in a PWR primary loop by using RELAP5/MOD3 for transient analysis. This study showed the effects of including support stiffness in piping analysis. This methodology showed a minimization of tank nozzle loads and damping factors.

A mathematical study proposed by Licsko et al. (2009) used a nonlinear ordinary first-order differential equation system to analyze the relief valve behavior. The study showed the appearance of an effect called Hopf Bifurcation, studied by Han and Bao (2009). It rises as inlet pressure gradually increases. If this pressure keeps increasing, it can lead to a chaotic behavior named grazing bifurcation.

Most of researchers showed the enormous number of variables that influences the valve stability and how complex and difficult it is to predict the behavior of the safety relief valve and the relation between each factor. But, as computer simulations have been used as a methodology to aid engineering design and performance assessment (Dominguez-Ontiveros & Hassan, 2009), the test of unviable situations becomes more accessible. As an example of this, Song et al. (2014) performed a transient numerical simulation using CFD methodology to show the difference between three vessel volumes during discharge. The study reported that the valve needs more time to blow down the same pressure difference for bigger vessels, when compared to minor vessels. It also reported a relation of pressure distribution inside the valve with the regulator ring position. The position of the regulator rings was also performed: the study showed that, as the distance between rings decreases, higher pressure distribution on the disc face is observed, producing higher flow forces. Minor forces on the disc allow the valve to close at higher vessel pressures. The study conducted by Song et al. (2014) showed the possibilities to analyze many situations in safety relief valves as an excellent non-intrusive method.

In conclusion, many factors influence a stable operation of the safety relief valve, not just the six major factors presented here, but a combinatorial analysis of all the circuit variables (Darby, 2013), leading to an extremely complex situation of predicting the main factor influencing the stability of the valve. But it is important to reinforce that the instability is not caused just by geometric factors, but also by the variations and relations that the process itself imposes on the valve, such as fluctuations in flow, waste deposits around the body, lack of maintenance, low boiler efficiency and lack of operator's capacitation.

Other studies can be conducted by using non-intrusive methods to analyze flow fields. Lasers have also been used to compare numerical and physical solutions for velocity field and mass flow rate according to different turbulence models. Laser techniques as DPTV and PIV have been used at Texas A&M University to benchmark velocity field for PWR fuel rods, and got good quality data according to Conner et al. (2013) and Dominguez-Ontiveros & Hassan (2014). Another example is the particle image velocimetry (PIV) for high speed in pipe elbows,

making possible the comparison between experimental and numerical analysis (Ono et al., 2011).

The present single-phase CFD study is based on mapping the intensity of outlet velocity, mass flow rate, discharge coefficient, maximum Mach number and disc forces using ANSYS-CFX® code. These physical quantities are compared to standards in order to verify if they are properly designed for industrial application.

2. Model development

A schematic cross-sectional view of the relief valve contemplated in this study is shown in Fig. 1 with the indication of the eight major components.

The mechanical operation of the safety relief valve is based on equilibrium forces acting on the disc. In order to keep the valve closed, the fluid force must be smaller than the force originated by the internal mass plus the spring force. To keep the valve open, the force imposed by the flow must be greater than the other forces mentioned in balance. When the sum is different from zero, the valve is not in mechanical equilibrium.

The internal pressure of the flow can be up to 10% higher than the set inlet pressure to reach the maximum lift, and may reach 10% lower than the set inlet pressure for the complete closure. Such non-linear behavior can be caused by several scaling factors according to Song et al. (2014). Therefore, several simulations will be carried out at steady-state condition to investigate the flow dynamics for an already open valve. So, the higher inlet pressure and backpressure effect originated in the opening or closing process will not affect the simulated geometry.

3. CFD analysis of SRV

A three-dimensional model was developed based on Fig. 1, using the finite volume method applied to a tetrahedral and prismatic unstructured mesh. The mathematical model considers the dry saturated steam flow in steady state condition and time averaging in the conservation equations for the following hypotheses: (i) Newtonian fluid and (ii) Buossinesq assumption for the Reynolds stresses. Thus, the average conservation equations for the mass, the momentum and energy are given respectively by Eqs. (1), (2) and (3).

All thermodynamic properties for dry saturated steam were evaluated as a function of temperature and pressure. This procedure is accomplished by the usage of a property table based on the International Association for the Properties of Water and Steam (IAPWS-IF97), and the appropriate formulation for the state equations used in this work is fully described at Wagner (1998).

$$\frac{\partial}{\partial x_j}(\rho U_j) = 0 \tag{1}$$

$$\frac{\partial}{\partial x_j}(\rho U_i U_j) = -\frac{\partial p}{\partial x_i} + \frac{\partial}{\partial x_j}(\tau_{i,j} - \rho\overline{u_i' u_j'}) \tag{2}$$

$$\frac{\partial}{\partial x_i}(\rho U_i h_{tot}) = \frac{\partial}{\partial x_i}\left(\lambda\frac{\partial T}{\partial x_i} + \frac{\mu_t}{\mathrm{Pr}_t}\frac{\partial h}{\partial x_i}\right) + \frac{\partial}{\partial x_j}[U_i(\tau_{i,j} - \rho\overline{u_i' u_j'})] \tag{3}$$

The flow in the valve has a highly compressible characteristic, thus, the work due to viscous stresses term $\frac{\partial}{\partial x_j}[U_i(\tau_{i,j} - \rho\overline{u_i' u_j'})]$ was considered. Reynolds stress tensor was calculated ($-\rho\overline{u}_i' u_j'$) according to the Boussinesq's hypothesis Eq. (4) and the shear stress ($\tau_{i,j}$) for a compressible gas can be expressed as indicated by Eq. (5). The effective viscosity (μ_{eff}), turbulent kinetic energy (k) and the mean total enthalpy (h_{tot}) are respectively shown at Eqs. (6), (7) and (8).

$$-\rho\overline{u_i' u_j'} = \mu_t\left(\frac{\partial U_i}{\partial x_j} + \frac{\partial U_j}{\partial x_i}\right) - \frac{2}{3}\delta_{i,j}\left(\rho k + \mu_t\frac{\partial U_k}{\partial x_k}\right) \tag{4}$$

$$\tau_{i,j} = \mu\left(\frac{\partial U_i}{\partial x_j} + \frac{\partial U_j}{\partial x_i}\right) - \frac{2}{3}\mu\delta_{i,j}\frac{\partial U_k}{\partial x_k} \tag{5}$$

$$\mu_{eff} = \mu + \mu_t \tag{6}$$

$$k = \frac{1}{2}\overline{u_i' u_i'} \tag{7}$$

$$h_{tot} = h + \frac{1}{2}U_i U_i + k \tag{8}$$

In the study of safety relief valves, the application of different turbulence models does not provide significant variation in the fluid behavior according to studies by Dempster and Elmayyah (2013). In addition, three turbulence models were tested: (i) the $k - \varepsilon$ model (Launder & Spalding, 1974), (ii) model $k - \omega$ (Wilcox, 1993), and (iii) Menter's SST k-ω (Menter et al., 2003).

Fig. 2 shows a graph for the mass flow through the valve for the tested turbulence models. All boundary conditions (such as pressure difference between inlet and outlet) were kept for all turbulence models.

Nevertheless, as the percentage change between the responses is relatively small, about 5% for the analyzed mathematical models, the $k-\varepsilon$ turbulence model has been chosen. The $k-\varepsilon$ model provides a better numerical stability and computational time. The use of the $k-\varepsilon$ model can also be considered a conservative choice, since it had the lowest value of the mass flow through the valve for the same pressure difference (Song et al., 2014).

The main objective of this paper was to obtain results for computational numerical simulations using a commercially available computational tool at the disposal of engineers and designers, and to compare the results with the ASME 2011a Section 1 standard, using the recognized good practices for discretization, choice of boundary

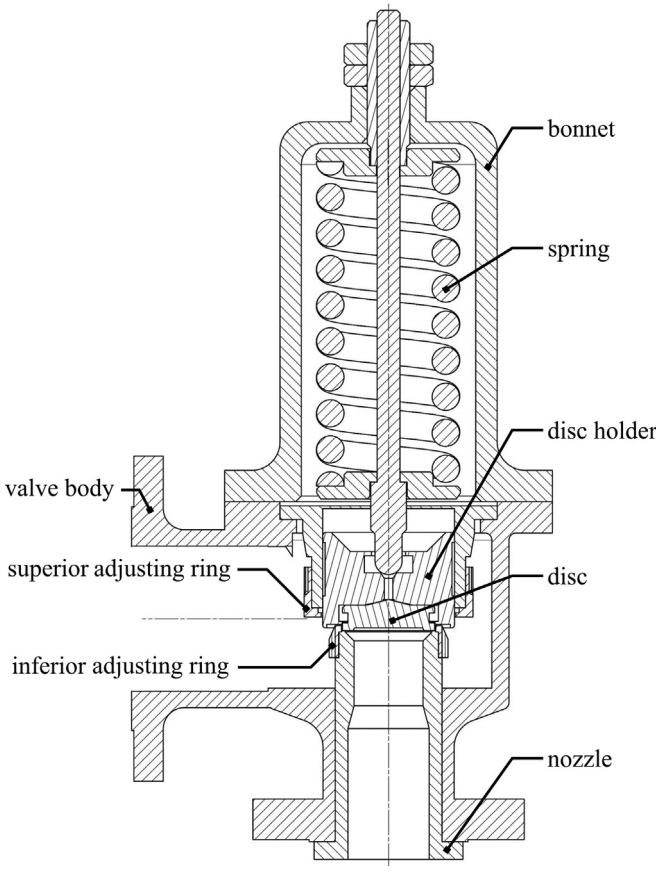

Fig. 1. Directly-operated SRV model.

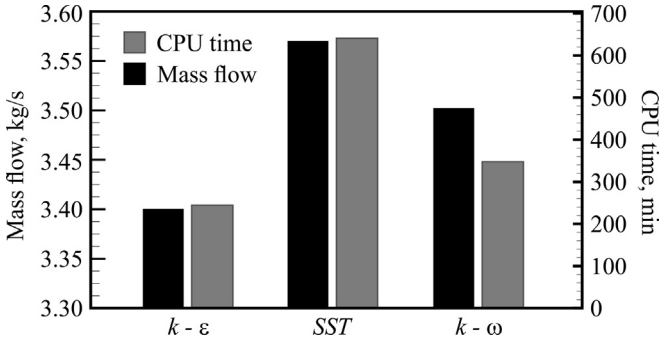

Fig. 2. CPU time and mass flow for different turbulence models.

conditions and fluid properties. In this sense, the proposed analysis does not include an extensive investigation of the response or limitations of the available turbulence model, which could only be done with a set of experiments properly conducted for this purpose.

The $k-\varepsilon$ turbulence standard model, one of the simplest and most famous turbulence models available (Ahsan, 2014), is widely used for the practical engineering flow problems solution Rolander et al. (2006). Thus, the expected conclusion is to recognize how the available simulation design tool responds against a well-established and disclosed simple algebraic mathematical mode of determination for relief valves.

The $k-\varepsilon$ two-equation turbulence model uses the gradient diffusion hypothesis to relate the Reynolds stresses to the mean velocity gradients and the turbulent viscosity (Ansys, 2008, 2006). The turbulent viscosity for this model is defined by Eq. (9), the calculations of turbulence kinetic energy (k) and turbulence dissipation rate (ε) come, respectively, from Eq. (10) and Eq. (11).

$$\mu_t = C_\mu \rho \frac{k^2}{\varepsilon} \tag{9}$$

$$\frac{\partial}{\partial x_j}(\rho \overline{U_j} k) = \frac{\partial}{\partial x_j}\left[\left(\mu + \frac{\mu_t}{\sigma_k}\right)\frac{\partial k}{\partial x_j}\right] + P_k - \rho\varepsilon \tag{10}$$

$$\frac{\partial}{\partial x_j}(\rho U_j \varepsilon) = \frac{\partial}{\partial x_j}\left[\left(\mu + \frac{\mu_t}{\sigma_\varepsilon}\right)\frac{\partial \varepsilon}{\partial x_j}\right] + \frac{\varepsilon}{k}(C_{\varepsilon 1} P_k - C_{\varepsilon 2}\rho\varepsilon) \tag{11}$$

The shear turbulent production (P_k) due to viscous forces where indicated at Eq. (12).

$$P_k = \mu_t\left(\frac{\partial U_i}{\partial x_j} + \frac{\partial U_j}{\partial x_i}\right)\frac{\partial U_i}{\partial x_j} - \frac{2}{3}\frac{\partial U_k}{\partial x_k}\left(3\mu_t \frac{\partial U_k}{\partial x_k} + \rho k\right) \tag{12}$$

3.1. Computational domain and spatial discretization

The computational domain is considered symmetrical, so as to reduce the required number of elements to be used without impairing the accuracy of the mathematical model. The existence of a complex secondary flow in outlet region is known, as rotational flow and cross flow through mid-plane. This simplification fails to capture those behaviors; however, the symmetrical consideration did not significantly influence the determination of mass flow through the valve or even the force exerted by the fluid on the disc.

Fig. 3 shows schematically an isometric view of the computational domain and indicates major regions of the device, which are: (i) inlet, (ii) nozzle, (iii) throat, (iv) disc, (v) outlet, (vi) increased domain. The increase in the downstream computational domain is an artificial strategy to ensure that all components of the velocity field, near to the outlet region, are pointed out of the computational domain, so as to avoid a numeric instability due to recirculation and heterogeneity in velocity field at this region.

The methodology used in this study aimed to verify the appropriate numerical mesh discretization, based on that proposed by Stern et al. (2001) and Wilson et al. (2001), where the error due to the discretization is minimized by a successive process solutions and refinements. The numerical solution is considered independent of discretization when the results, for the same boundary conditions, have insignificant variation with the increase of the number of elements.

Fig. 4 shows a graph for various physical quantities (mass flow, average outlet velocity, average outlet static pressure, average outlet density) as a function of the number of elements, for the same boundary conditions. The dotted line in this figure indicates that, beyond this line, the quantities remain almost constant, so that the final mesh was set with 3.4 million elements. Fig. 5 also shows the relative mesh volume and distribution used in $k-\varepsilon$ turbulence model. Mesh counts with body sizing of maximum edge length with 2 mm, and 0.8 mm for all internal faces near the throat area.

3.2. Boundary conditions

The summary of the boundary conditions is listed below:

(i) Average outlet pressure equal to 1 bar (absolute);
(ii) Inlet pressure ranging from 0.3 MPa to 1.3 MPa (0.3, 0.5, 0.7, 0.9, 1.1 and 1.3 MPa);
(iii) Inlet temperature equal to the saturation temperature for the inlet working pressure;
(iv) The logarithmic wall function is used (Launder & Spalding, 1974) and the profile is corrected to incorporate fluid compressibility effects (Huang et al., 1993), using an equivalent roughness of all internal surfaces equal to 0.2 mm according to the valve design.
(v) Symmetry boundary condition in plane xz, Fig. 3;
(vi) Nozzle opening (a) ranging from 3 mm to 18 mm (3, 6, 9, 12, 15 and 18 mm).

The combination of the conditions *ii* and *vi* resulted in thirty-six simulations. For the first boundary condition, the flow is considered subsonic in the outlet surface, which requires a predefined pressure

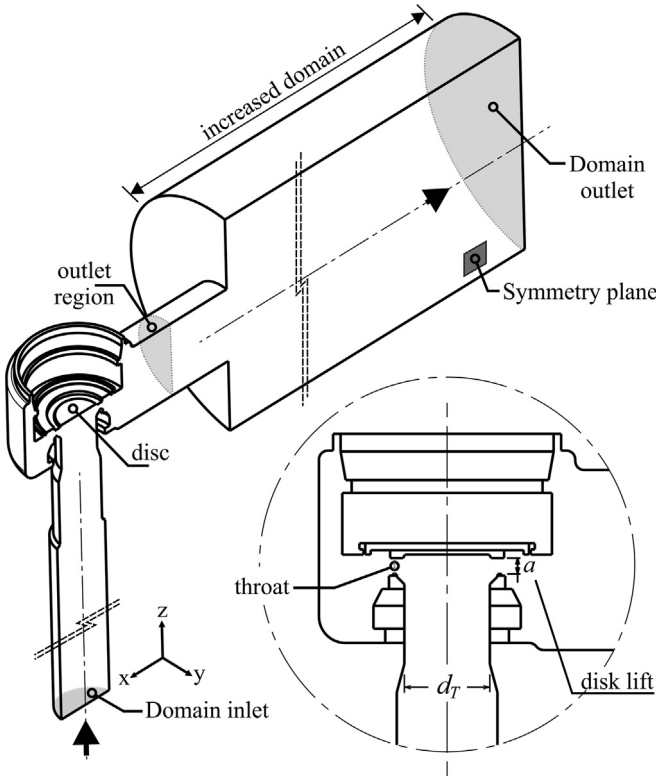

Fig. 3. Isometric view of the domain and nomenclature for principal regions.

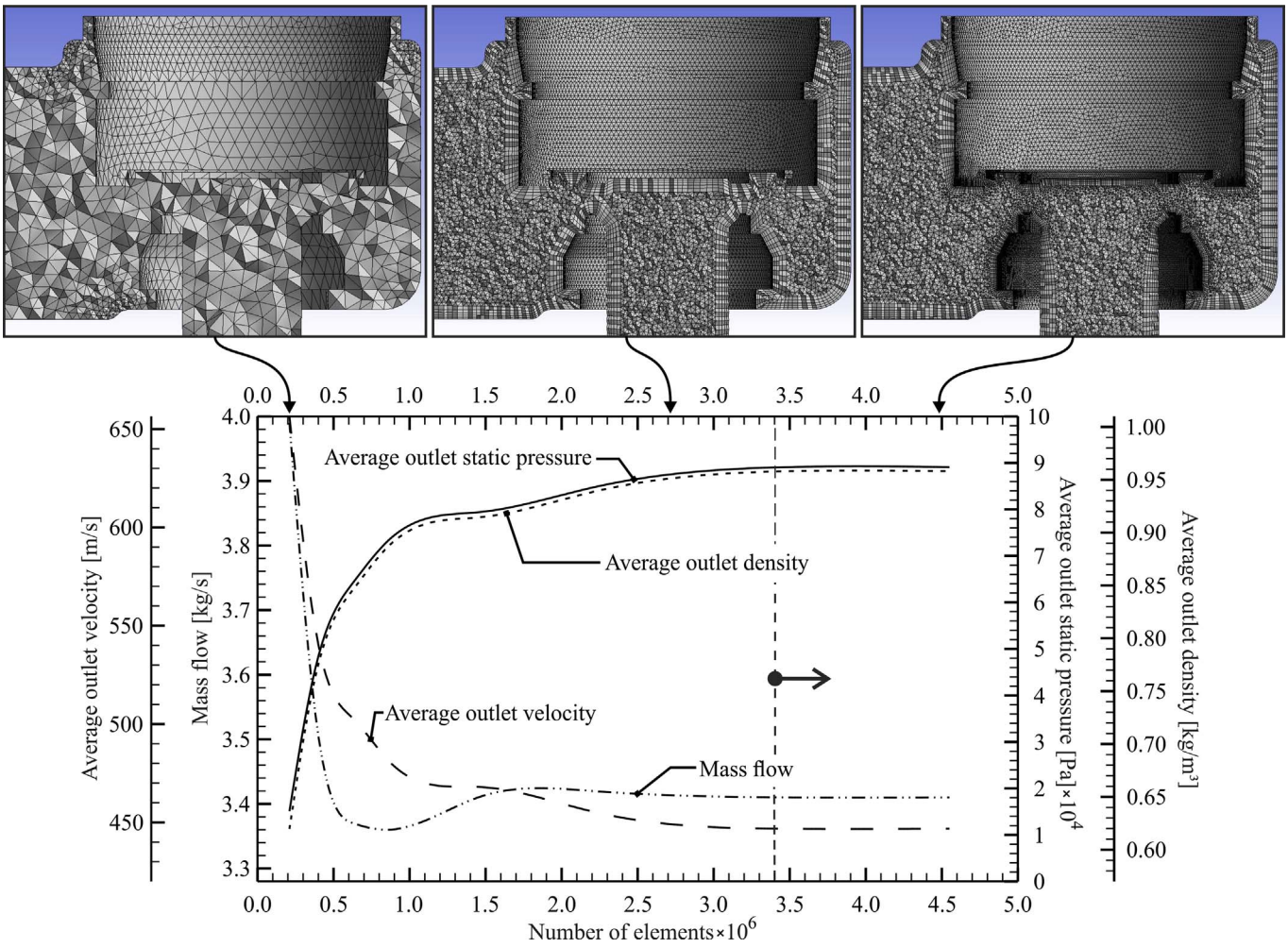

Fig. 4. Number of elements as a function of mass flow, average outlet velocity, average outlet density and average outlet pressure.

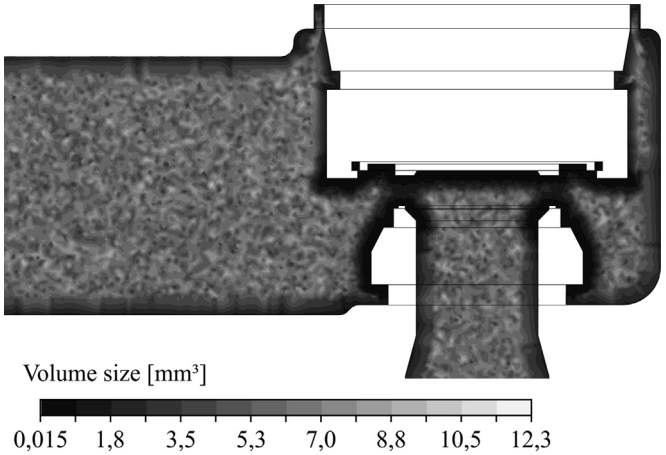

Fig. 5. Relative mesh volume for 3.4 million of elements designed for k-epsilon turbulence model.

value. However, when the flow reaches sonic or supersonic velocity near the throat area, the outlet condition needs to be changed to supersonic outlet and the outlet pressure value is no longer necessary. The detailed description of this mathematical behavior can be obtained for nozzle studies by Anderson (2002). Mathematically, these two flow possibilities, subsonic and supersonic, impact on the mathematical behavior of the conservation equations, changing the solution from elliptic to hyperbolic. In order to avoid mathematical inconsistencies, the length of the outlet pipe has been increased to guarantee subsonic outlet.

3.3. Solver options and convergence criteria

The high-resolution implicit total variation diminishing (TVD) model showed an improvement in shock-capturing schemes, either for steady or unsteady calculations (Yee et al., 1990). These schemes showed to be an efficient discretization method and sufficiently accurate for very complex hypersonic inviscid and viscous shock interactions. So, the same type of high-resolution scheme was used in simulations as advection and turbulence scheme discretization.

All steady simulations were performed with spatial convergence errors lower than 10^{-5} for root mean square (RMS) for the mass, momentum, energy and turbulence.

3.4. Numerical validation

In the computational domain, under supersonic conditions, it is possible to observe values of Mach number greater than one ($M > 1$). In such conditions, an intense gradient in physical properties should be observed, which would indicate the existence of a shockwave.

A validation test was conducted to verify the ability of the solver to adequately predict shockwave formation, position and intensity of the physical phenomenon. The test was performed for a transonic air flow through a converging-diverging diffuser geometry due to an extensive experimental data provided and a wide range of the flow conditions

(Chen et al., 1979; Sajben et al., 1981; Bogar 1986; Bogar et al., 1983; Salmon et al., 1983). The geometry of the convergent-divergent was generated according to the equation presented by Bogar et al. (1983).

A three-dimensional model for the transonic diffuser was developed based on the finite volume method applied to an unstructured mesh in a steady state condition. The mass, the momentum and energy conservation equations are considered. The turbulence models used are the same ones presented in the valve case. The mesh was verified individually for each turbulence model according to Stern et al. (2001) and Wilson et al. (2001) criteria.

The air was considered as calorically-perfect gas and Sutherland's law (Sutherland, 1893) was used for the viscosity correction with temperature. The boundary conditions applied to the validation test are schematically indicated at Fig. 6 and listed below:

(i) subsonic inlet with total absolute pressure equal to 135 kPa and temperature equal to 300 K;
(ii) outlet static pressure equal to 101.8 kPa_{abs};
(iii) no-slip wall condition for upper and lower surfaces; and
(iv) two symmetry conditions (planes α and β).

The use of symmetry on both side surfaces is required since ANSYS-CFX® is not able to solve purely two-dimensional problems.

Fig. 7 presents the results obtained by simulations compared to the experiments (Sajben et al., 1981). The comparison is performed for a horizontal line located on the lower surface of the computational domain, with y = 0 in the Cartesian system positioned according to Fig. 6. In Fig. 7, the length (x) and absolute pressure (p) was normalized, where h_T (40 mm) is the throat height and p_0 an absolute reference pressure (135 kPa).

Analyzing Fig. 7, it was possible to verify that the solver can capture the existence of the shockwave independently of the turbulence model used. It was noticed that among the turbulence models, the Shear Stress Transport model predicted more adequately the phenomenon, presenting an absolute error of 7% for the shockwave position ($x/h_T = 2.413$) while $k-\varepsilon$ (10.5%, $x/h_T = 2.492$) and $k-\omega$ (15.7%, $x/h_T = 2.609$) delay the formation of the shockwave.

Fig. 8 presents a contour map for each tested turbulence model, indicating the normalized absolute static pressure. In this figure, it is possible to notice an abrupt pressure variation in the shockwave position.

4. Results

4.1. Average outlet velocity

The first behavior that indicates consistency in the results is observed in Fig. 9. In this figure, the average outlet velocity as a function of the throat opening for different inlet pressures is shown. The increase in the inlet pressure results in an increase in the average outlet velocity. However, for the same inlet pressure, the increase of the throat opening results in a velocity increase for opening values of less than 12 mm and becoming almost constant from beyond this point.

The behavior shown in Fig. 10 can be justified by observing the three main regions of the flow passage:

- Domain inlet area (A_{IN}), coincident with the valve inlet area;
- Outlet region area (A_{OUT}), previously shown in the Fig. 3 and equal to the outlet area of the valve;
- Throat area (A_T), flow area formed between nozzle and disc.

Eq. (13) indicates the approximate throat area. This equation neglects the effects of *vena contracta* formed in the region of the throat. The flow area in this region is assumed as the lateral area of a cylinder.

$$A_T = \pi \cdot d_T \cdot a \tag{13}$$

where, d_T is the inlet throat diameter and a is the disc lift.

Fig. 10 shows the behavior of the throat area towards inlet and outlet areas. It was found that, with the increase of the disc lift (a), the throat area tends to be equal to the inlet area. This occurs for disc lift equal to 14.25 mm.

It is observed that, for openings smaller than 14.25 mm ($a < 14.25$ mm), the mass flow through the valve is limited by the throat area. If the throat area is greater than the inlet area, the mass flow through the valve is limited by the valve inlet region. This characteristic justifies the behavior of the constant average outlet velocity for a disc lift higher than 12 mm.

4.2. Mass flow

ASME 2011a Section 1 provides standards for relief and pressure valves for the calculation of the theoretical flow for both smaller openings ($A_{IN} > A_N$) and bigger openings ($A_N > A_{IN}$). In ASME 2011a standards, the mass flow calculation (theoretical condition) for smaller openings is classified as "Flat Seat", and the one for bigger openings is classified as "Nozzle".

The mass flow calculations for the Flat Seat and Nozzle conditions are respectively indicated in Eqs. (14) and (15).

$$\dot{m}_S = 5{,}25 \cdot A_T p_{IN} \tag{14}$$

$$\dot{m}_S = 5{,}25 \cdot A_{IN} p_{IN} \tag{15}$$

where, p_{IN} is the inlet pressure (SI).

Fig. 11 shows a comparison between the theoretical mass flow rate calculated by the standard and mass flow rate obtained by the simulation. It is important to note that the same behavior observed in average outlet velocity is verified for mass flow. It is also possible to observe that in all simulated cases, the mass flow for the same inlet pressure is lower than that calculated by the standards. This behavior is also expected since mechanical energy losses are not considered in Eqs. (14) and (15).

4.3. Discharge coefficient

Calculations of the valve discharge coefficient were based on the ASME 2011a formulation, Eq. (16). The real mass flow rate ($\dot{m}_R$) was obtained by the simulations and standards mass flow ($\dot{m}_S$) according to Eqs. (14) and (15).

$$k_d = \dot{m}_R / \dot{m}_S \tag{16}$$

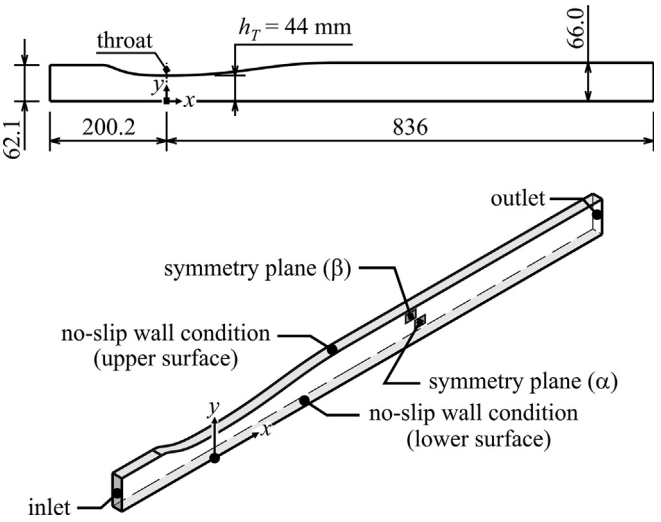

Fig. 6. Indication of the principal dimensions in millimeters of the convergent-divergent geometry and boundary conditions.

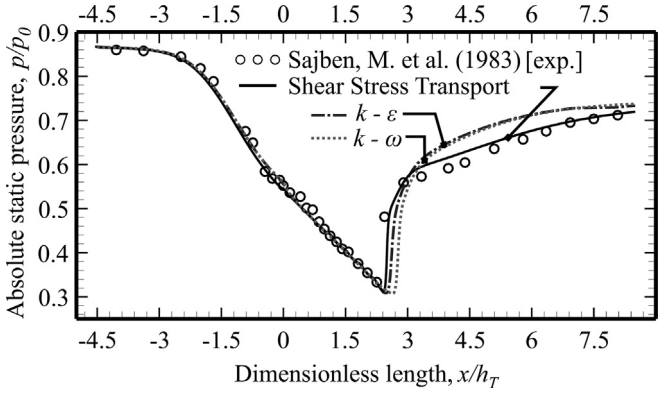

Fig. 7. Pressure variation as a function of length on the lower surface of the computational domain.

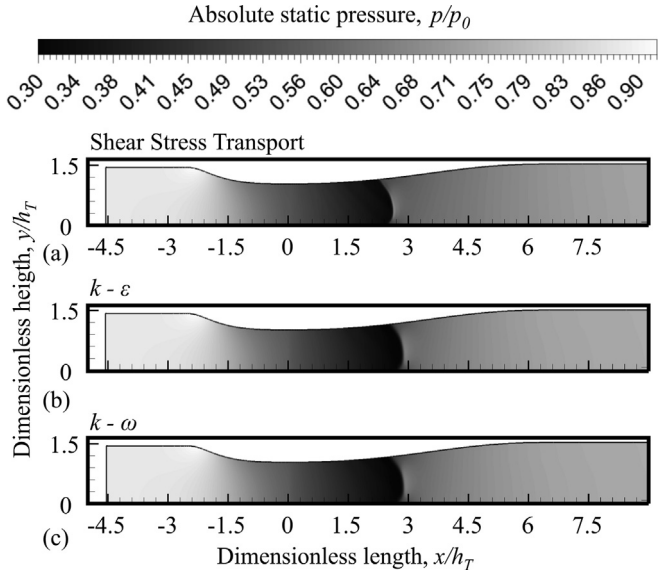

Fig. 8. Contour map indicating absolute static pressure (p/p_0) for: (a) Shear Stress Transport; (b) k–ε and (c) k–ω.

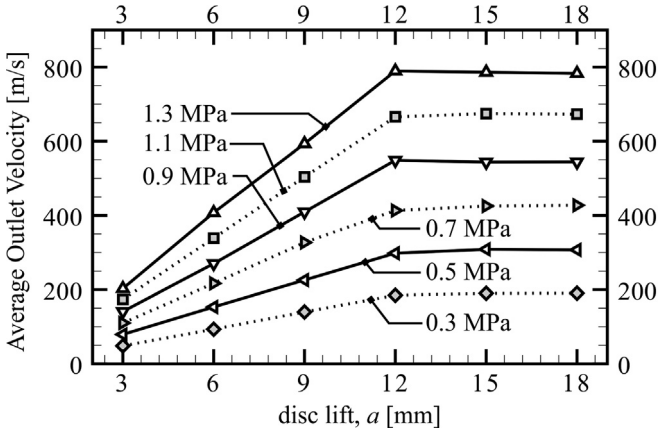

Fig. 9. Behavior of the average outlet velocity in function of the disc lift (a) for each simulation.

Values for the discharge coefficient as a function of the disc lift are shown in Fig. 12. The bars indicate the maximum and minimum dispersion in the discharge coefficient for the same disc lift. The average values of the discharge coefficient ($\overline{k_d}$) are indicated in Table 1. This table also shows the standard deviation (σ) and the maximum deviation defined by Eq. (17).

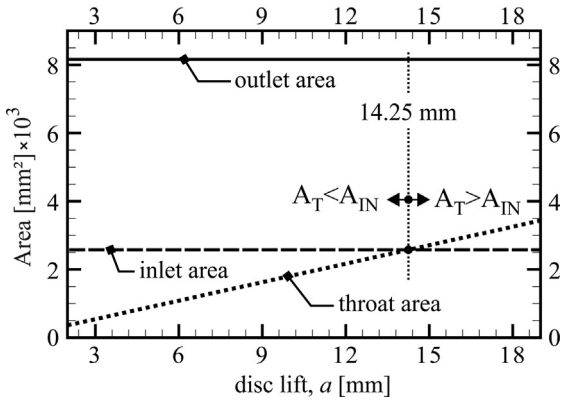

Fig. 10. Comparison between inlet area, outlet area and throat area as a function of the disc lift.

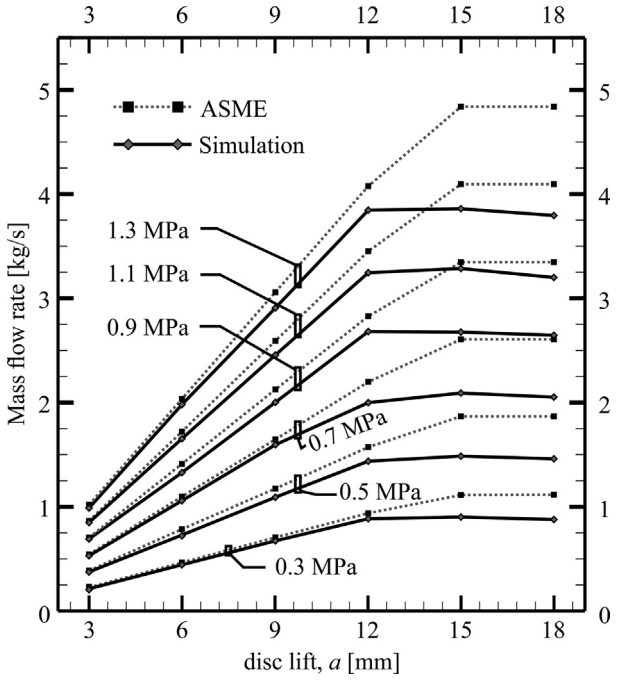

Fig. 11. Mass flow rate as a function of disc lift.

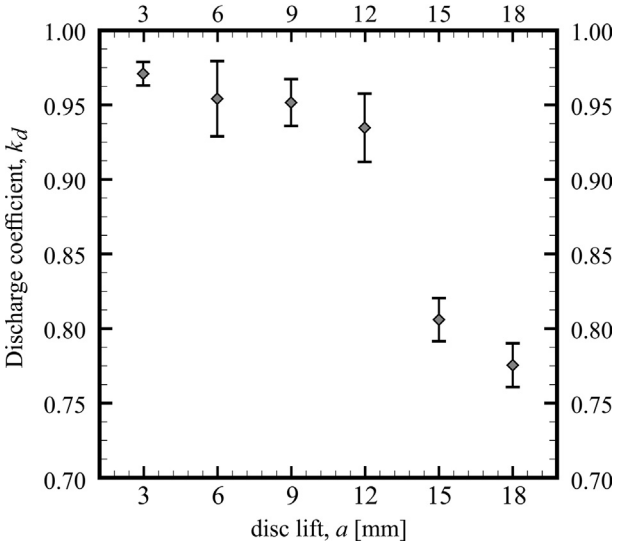

Fig. 12. Discharge coefficient as a function of the disc lift.

Table 1
Average discharge coefficient, standard deviation and maximum deviation as a function of the disc lift.

a [mm]	$\overline{k_d}$	σ	δ_{MAX} [%]
3	0.975	0.00609	1.64
6	0.957	0.01799	5.07
9	0.951	0.01234	3.14
12	0.939	0.01719	4.79
15	0.803	0.01081	3.52
18	0.773	0.01092	3.62

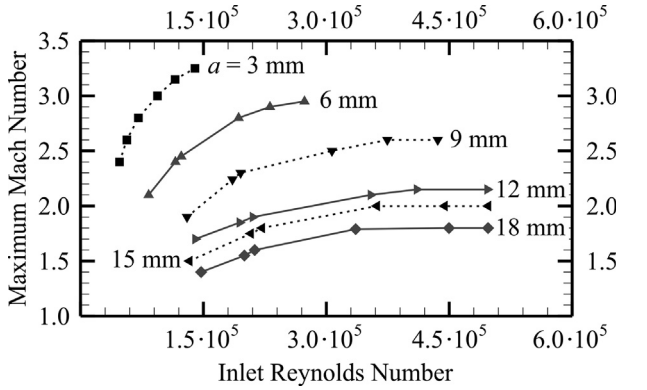

Fig. 13. Maximum Mach number in the computational domain as a function of the inlet Reynolds number.

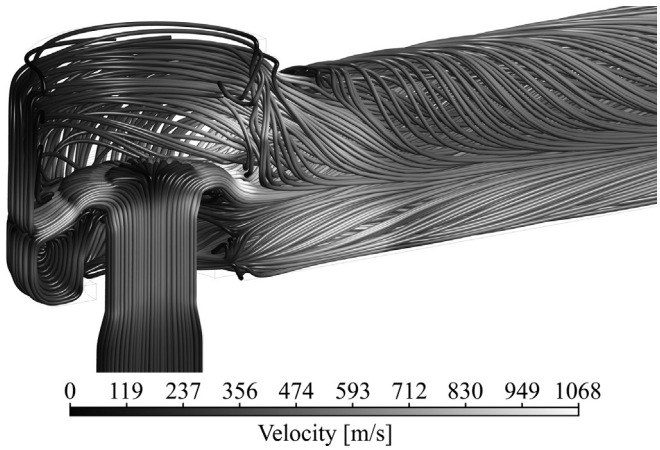

Fig. 14. Streamlines at full lift and pressure.

$$\delta_{MAX} = \frac{\dot{m}_{R(max)} - \dot{m}_{R(min)}}{\dot{m}_{R(max)}} 100 \quad (17)$$

Considering all the uncertainties in this study, the values showed similarities with studies carried out by Kim et al. (2006) and Schmidt et al. (2009) for the discharge coefficients. However, some particularities should be briefly discussed, such as the maximum deviation behavior observed for each valve opening. Between the total opening (18 mm) up to 9 mm, there were no large variations of the maximum deviation, however, for 6 mm, it reached 5.07%, followed by the minimum statistical value (1.64%). Among the possibilities, it is believed that the position of the regulation rings has a delicate influence on the smaller openings, because, as discussed in item 4.6, the 6 mm aperture obtained the largest portion of force transmitted to the disc.

4.4. Mach number

Average values were obtained for the calculation of some quantities such as velocity, density, pressure. However, their maximum and minimum values were not computed, since it is out of the scope of this study.

In this case, obtaining the maximum values of the Mach number is of great interest, since this value exhibits the valve behavior. Mach average values for the outlet region in the valve can hide a possible supersonic behavior.

To verify the existence of shockwaves, Fig. 13 indicates the maximum Mach number in the complete computational domain according to the inlet Reynolds number.

Fig. 14 shows streamlines behavior nearby the throat area. The existence of higher velocity profiles, coupled with generation of large turbulent frequencies, prevails in the downstream to the throat area. This behavior is known and widely reported by Kasai (1968). This recirculating structure promotes instability behavior on the discs experimentally demonstrated by Hős et al. (2014). Depending on the magnitude due to collisions between disc and valve seat, according to Vu et al. (1994), the instability can cause premature wear.

4.5. Shockwave

Even if the flow does not behave as a purely one-dimensional flow, a simple analysis of the average general behavior of the flowing fluid reveals a peculiar pattern. Fig. 15 indicates a graph constructed for a vertical line from the valve inlet to the center of the disc. It is not the analysis of a streamline, but a generic analysis of some flow properties of interest in that region. In Fig. 15 it is possible to observe, in the flow direction, the initial Mach number in the region where there is the first decrease of the diameter (alpha region indicated in Fig. 17 and Fig. 18). Being a subsonic flow, the area reduction really should lead to an acceleration of the fluid, as observed. Subsequently, a second area reduction (beta region indicated in Fig. 17 and Fig. 18) again increases fluid velocity. The complex feature of the three-dimensional flow begins to be noted just upstream of the section “x-x” to the valve disc region. The central flow in the latter region results in a Mach number decrease (because of the valve disc), which can configure the presence of a shockwave. The results of the mathematical model indicate a dispersion of this shockwave that looks like a bowl shape, located in a detached position and in front of the valve disc. The more peripheral flow in the region of section “x-x” remains sonic, showing an increase in the area caused by the geometry of the valve in this region, as a function of chamfer (with the possible presence of Prandtl Meyer expansion waves), which allows supersonic fluid velocity. In sequence, radial flow (and increasing areas) further accelerates the supersonic vapor.

A horizontal line, also constructed for flow analysis, is shown with quantities of interest indicated in Fig. 16**.** The radial acceleration of the fluid is locally influenced by the geometric details on the valve disc (grooves), though, after passage of the fluid by the region with the grooves, there is a continuous increase in the Mach number to the region after the disc where the valve diameter is constant, which tends to equalize the flow quantities.

The Mach equal to one should occur in the section of the throat of the valve (lower area between the valve seat and the disc), admittedly the section with smaller area in the flow. However, the presence of the disc and the possible shockwave, imposed a restriction, forced a three-dimensional flow pattern, causing an unexpected and atypical central hydraulic block, advancing the smallest flow area (real geometric throat area) to a virtual throat area located upstream of the actual geometric throat area. A phenomenon comparable to a kind of *vena contracta*. Thus, the pressure distribution on the disc front is lower than the one obtained if the flow is without the shockwave detached presence, and the anticipation of the smaller area of free flow for a section downstream valve, justifying the lowest force disc results found in the simulations (results compared to the empirical model).

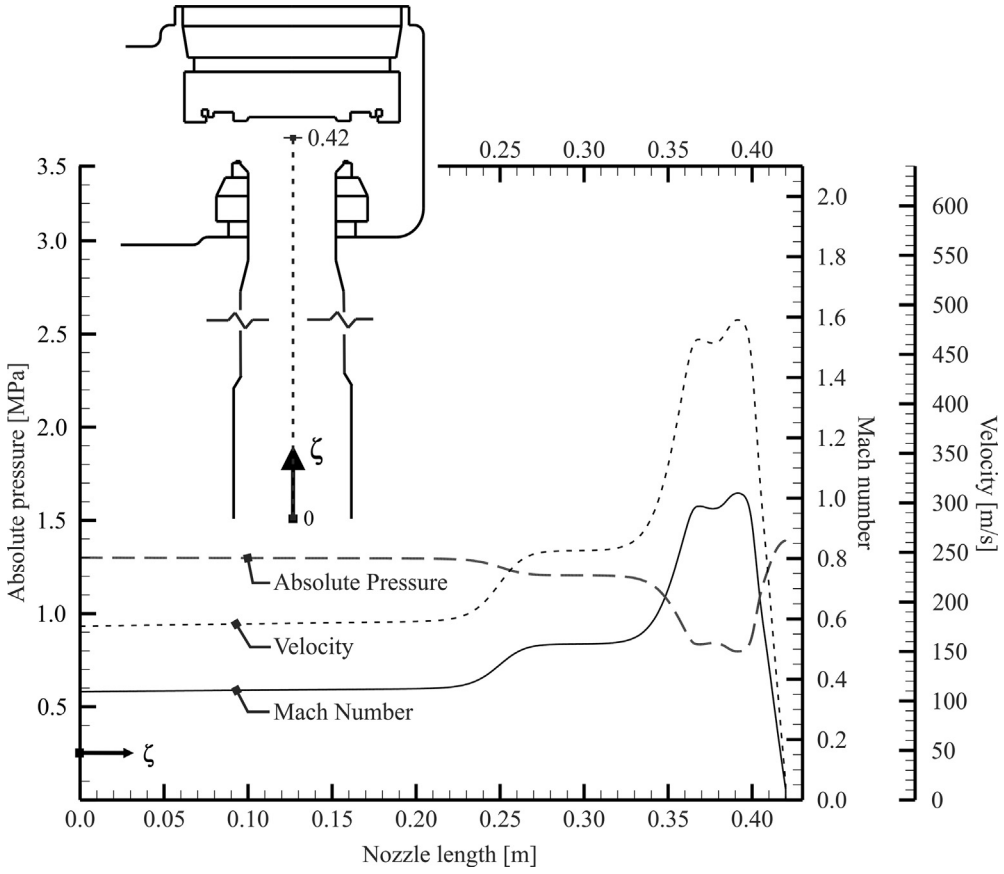

Fig. 15. Physical properties in vertical line (zeta line).

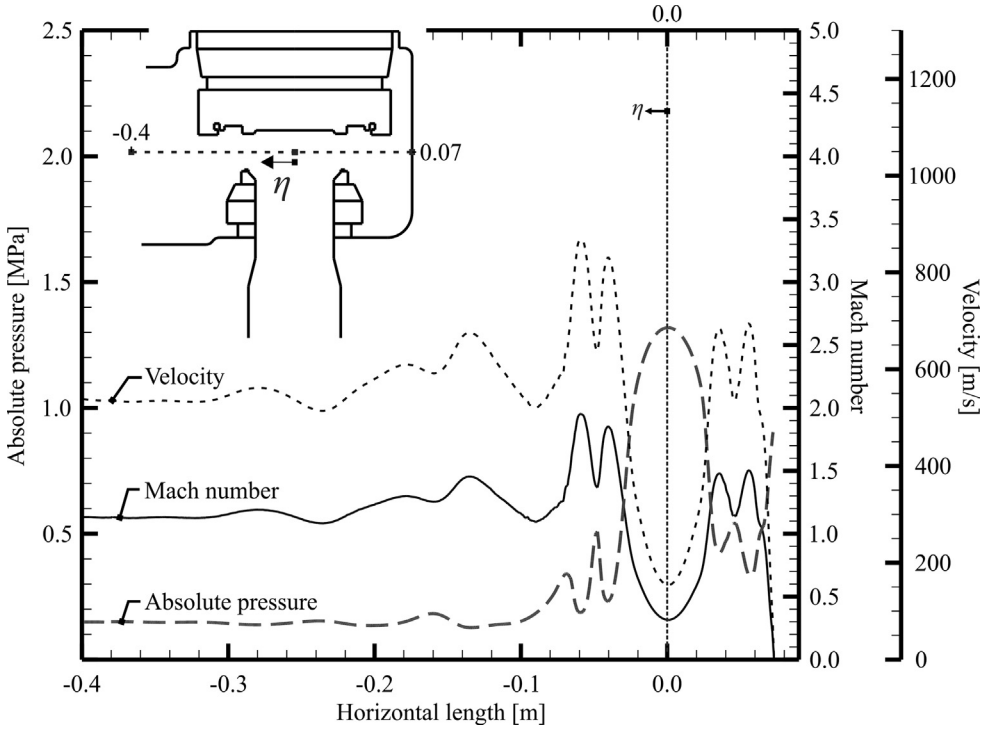

Fig. 16. Physical properties in horizontal line (eta line).

4.6. Disc force

The conventional manner to determine the force applied on the disc is to convert all the work done by the pressure at the inlet into a normal force applied on the disc. It does not consider vortex formations and neglects any other three-dimensional behavior of the flow, regardless of the flow conditions. The force obtained by this procedure is used to calibrate the opening/closing condition, which is used in the spring design. However, this procedure implies that the force acting on the disc for the same inlet pressure remains constant.

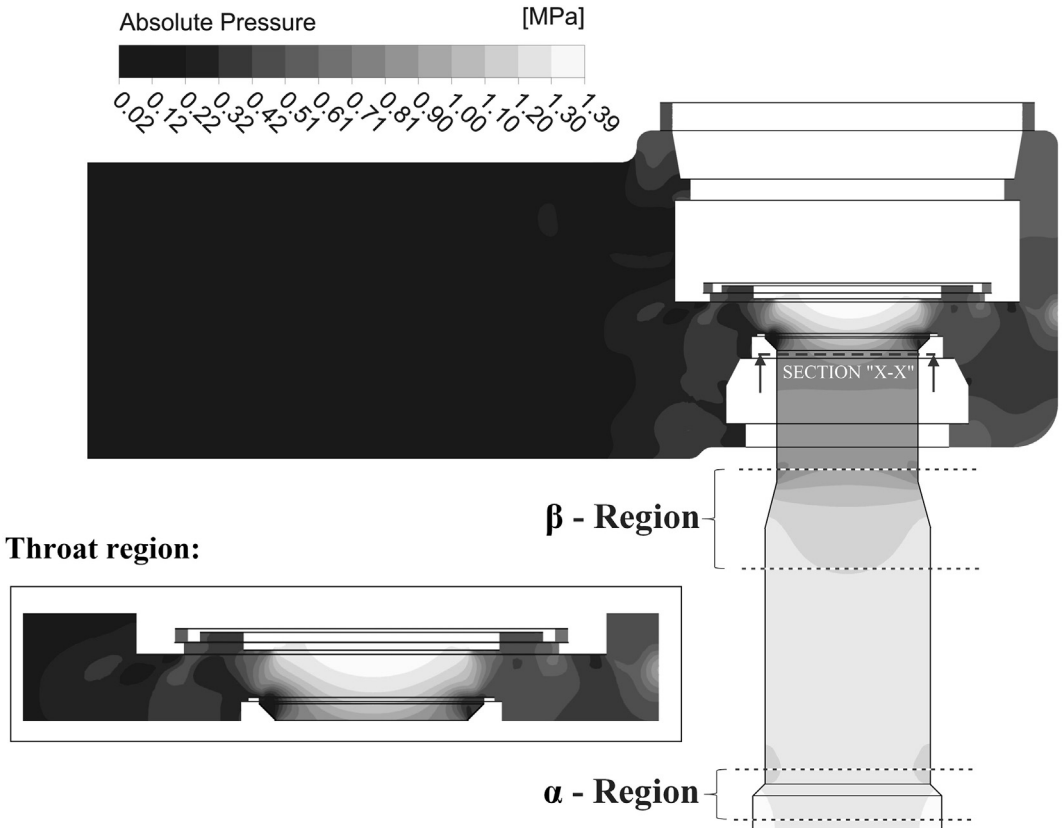

Fig. 17. Gray map for absolute pressure in symmetrical plane.

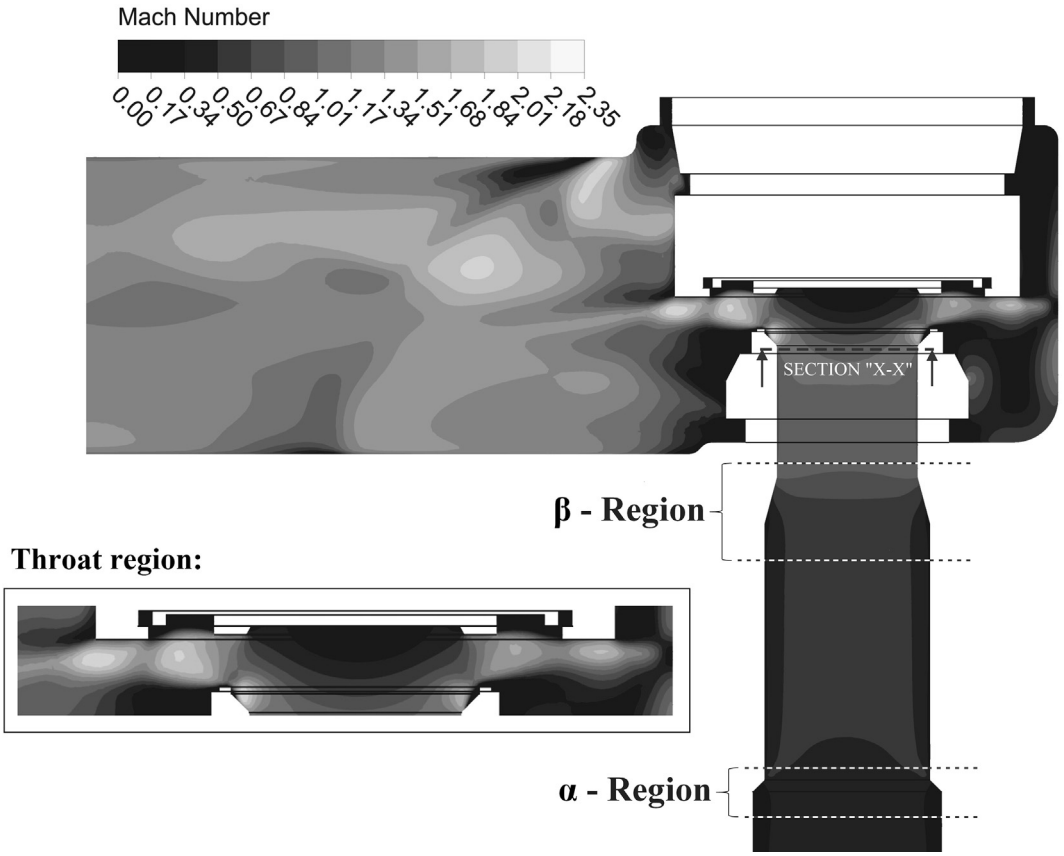

Fig. 18. Gray map for Mach number in symmetrical plane.

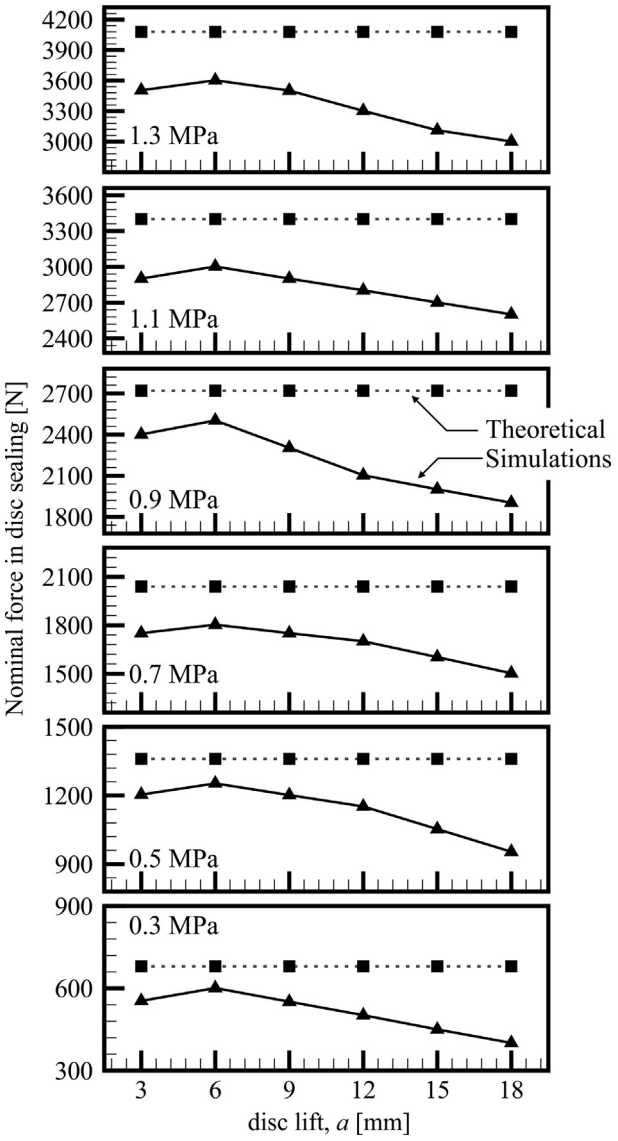

Fig. 19. Normal force at the disc sealing.

Fig. 19 presents a comparison between the normal force on the disc sealing by the theoretical condition, which considers that all static inlet pressure is converted into mechanical work in the disc area, and the force obtained by the simulation as a function of the disc lift. Fig. 19 was separated into groups, to facilitates the visualization according to the inlet pressure. This figure also revealed that the force acting on the disc presents a non-linear behavior and cannot be considered constant. It is possible to observe that the magnitude of the inlet pressure does not matter. For a given disc lift, the force transmitted to the sealing disc is always lower than the theoretical value.

This study can support the spring design analysis in pressure relief valves in order to avoid oversizing. It is known that an incorrect spring selection can cause intense vibrational behavior or the valve remains closed at the design condition (Bazsó and Hös, 2013).

Fig. 19 shows an interesting behavior for each opening. Starting from a 3 mm opening, the transmitted mechanical force portion grows to a peak at 6 mm, decreasing linearly up to a 18 mm opening. This behavior may be tied to the position of the adjusting rings, where, for minimum openings, both rings remain near to each other, increasing the area with which the fluid can convert its kinetic energy to mechanical. However, for larger openings, the superior adjusting ring become far away from nozzle, reducing the force transmitted to the disc. The CFD simulations showed that average normal disc force is about 19% lower than theoretical ASME force, which could prevent the valve oversizing.

5. Conclusions

A three-dimensional numerical study is presented for a security relief valve using the ANSYS-CFX® commercial code. The study mapped various physical situations – particularly, the transonic and supersonic conditions.

The mathematical model considered steady state flow and included dry saturated steam at extremely compressible condition. All thermodynamic properties were corrected International Association for the Properties of Water and Steam. The discretization of the computational domain was appropriately analyzed using recommended techniques in scientific and technical literature.

This study, conducted in accordance with several opening positions and inlet pressure conditions, resulted in 36 steady state simulations. To obtain the transonic and/or supersonic behavior, the increment of the outlet domain allows the use of a subsonic boundary condition for the outlet. It allows the model to capture all the phenomena inside the valve using the same outlet boundary conditions, including a possible shockwave condition.

One of the properties responsible for predicting relief valve behavior efficiency is the discharge coefficient. As shown in item 4.2, the valve presented coefficients and mass flow according to the ASME 2011a Section 1 safety standard.

Due to the number of Mach reaching high values in certain simulations ($M > 0.7$), the turbulence originated by transonic and supersonic situations could induce vibrations in the disc, which could affect stability of the valve, as shown by Bardina et al. (1997).

The minimum flow area, according to the results of the simulations, was anticipated, not corresponding to the smaller flow area between the disc and the valve seat, an effect possibly caused by the presence of the disc (central flow restriction causing a possible bowl-shaped shockwave) of the valve and a small divergent anterior to the seat region, forming a specimen of the *vena contracta*.

The relief valve operated by spring requires several adjustments at the time of installation, which must be in accordance with the respective standard. Nuclear and industrial hydraulic circuits operate with different patterns and variations. Working with steam, PWR and BWR nuclear reactors have their physical quantities constantly monitored, and their variation must be predicted to guarantee safety operation.

The factors that may alter significantly the operation of the valve are presented in item 1, where: Valve design (Kasai, 1968); Spring predeformation (x) (Bazsó & Hös, 2013); Length of the inlet pipe line (L), (Thomann, 1976); Valve opening length (δ) (Song et al., 2014) and (Singh, 1982); Regulator rings position (x') (Green & Woods (1973); and Pressure vessel volume (ϑ) (Song et al., 2014). These six variables are defined as the most critical in its operation.

As studied by Bazsó and Hös (2013), it is impossible to get a "perfect valve adjustment" where the valve will not result in vibrations and instabilities by such many variables. It is important to mention that valve maintenance and testing practices influence directly the valve behavior, McElhaney (2000).

As the most influential variable, the course of the disc was the major object of this study; all the other variables were kept constant. Theoretical analysis showed a critical behavior in the 14.25 mm opening, which would present an equality between the inlet area and throat area, thus providing a constant behavior after this opening. Simulations showed this behavior for lift smaller than 12 mm. It could help in the discharge coefficient design and also avoid errors during hydraulic sizing.

The vibrational elements were compared to Francis & Betts (1998) and Green & Woods (1973) papers to determine similarities with the

relief valve of this study. The mathematical model used by Darby (2013) assisted in the prediction of studied factors such as the vibrational behavior of the valve. So, the presence of high rotational eddy at Fig. 14 could indicate instabilities (Galbally et al., 2015).

Although this CFD study has not been validated experimentally, a numerical validation has been compared to extensive experimental data provided and a wide range of the flow conditions (Chen et al., 1979; Sajben et al., 1981; Bogar, 1986; Bogar et al., 1983; Salmon et al., 1983). The numerical code proves to be capable of predicting shockwave phenomena as illustrated in Fig. 17 and Fig. 18 for safety relief valve and Fig. 8 for the converging-diverging diffuser geometry. Other studies also achieved similar results for wave formations for relief valve using CFD methodology (Bassi et al., 2011, 2014). An important study also revealed the shockwave formations after safety/relief valve discharge (Moody, 1982).

Acknowledgments

The authors would like to acknowledge the Nuclear and Energy Research Institute, IPEN-CNEN/SP, for allowing the use of its infrastructure, particularly the computer laboratory.

References

Ahsan, M., 2014. Numerical analysis of friction factor for a fully developed turbulent flow using k-epsilon turbulence model with enhanced wall treatment. Beni-Suef Univ. J. Basic Appl. Sci. 3 (4), 269–277.
Anderson, J., 2002. Modern Compressible Flow: With Historical Perspective, third ed. McGraw-Hill Education, s.l.
Ansys, 2008. ANSYS CFX-Pre User's Guide, 15.0 ed. Ansys, Canonsburg.
Ansys, C., 2006. Solver Theory Guide. Ansys CFX Release, Issue 2006.
Bardina, J., et al., 1997. Turbulence Modeling Validation. National Aeronautics and Space Administration, pp. 1–100.
Bassi, F., et al., 2011. High-order discontinuous Galerkin computation of axisymmetric transonic flows in safety relief valves. Comput. Fluids 49 (1), 203–213.
Bassi, F., et al., 2014. Investigation of flow phenomena in air–water safety relief valves by means of a discontinuous Galerkin solver. Comput. Fluids 90, 57–64.
Bazsó, C., Hös, C.J., 2013. An experimental study on the stability of a direct spring loaded poppet relief valve. J. Fluids Struct. 42, 456–465.
Bogar, T., 1986. Structure of self-excited oscillations in transonic diffuser flows. AIAA J. 24 (1), 54–61.
Bogar, T., Sajben, M., Kroutil, J., 1983. Characteristic frequencies of transonic diffuser flow oscillations. AIAA J. 21 (9), 1232–1240.
Botros, K.K., Dunn, G.H., Hrycyk, J., 1997. Riser-relief valve dynamic interactions. J. Fluids Eng. 119 (3), 671–679.
Chabane, S., et al., 2009. Vibration and chattering of conventional safety relief valve under built up back pressure. In: 3rd IAHR International Meeting of the WorkGroup on Cavitation and Dynamic Problems in Hydraulic Machinery and Systems, pp. 281–294.
Chen, C., Sajben, M., Kroutil, J.C., 1979. Shock-wave oscillations in a transonic diffuser flow. AIAA J. 17, 1076–1083.
Conner, M.E., Hassan, Y.A., Dominguez-Ontiveros, E.E., 2013. Hydraulic benchmark data for PWR mixing vane grid. Nucl. Eng. Des. 264, 97–102.
Darby, R., 2013. The dynamic response of pressure relief valves in vapor or gas service, part I: mathematical model. J. Loss Prev. Process Ind. 26 (6), 1262–1268.
Dempster, W., Elmayyah, W., 2013. Two phase discharge flow prediction in safety valves. Int. J. Press. Vessels Pip. 110, 61–65.
Dominguez-Ontiveros, E.E., Hassan, Y.A., 2009. Non-intrusive experimental investigation of flow behavior inside a 5 × 5 rod bundle with spacer grids using PIV and MIR. Nucl. Eng. Des. 239 (5), 888–898.
Dominguez-Ontiveros, E., Hassan, Y.A., 2014. Experimental study of a simplified 3 × 3 rod bundle using DPTV. Nucl. Eng. Des. 279, 50–59.
Francis, J., Betts, P.L., 1998. Backpressure in a high-lift compensated pressure relief valve subject to single phase compressible flow. J. Loss Prev. Process Ind. 11 (1), 55–66.
Funk, J.E., 1964. Poppet valve stability. J. Basic Eng. 86 (2), 207–212.
Galbally, D., et al., 2015. Analysis of pressure oscillations and safety relief valve vibrations in the main steam system of a Boiling Water Reactor. Nucl. Eng. Des. 293, 258–271.
Green, W.L., Woods, G.D., 1973. Some causes of chatter in direct acting spring loaded poppet valve. In: The 3rd International Fliud Power Symposium. Turin.
Han, W., Bao, Z., 2009. Hopf bifurcation analysis of a reaction–diffusion Sel'kov system. J. Math. Anal. Appl. 356 (2), 633–641.
Hayashi, S., Hayase, T., Kurahashi, T., 1997. Chaos in a hydraulic control valve. J. Fluids Struct. 11 (6), 693–716.
Hős, C.J., Champneys, A.R., Paul, K., McNeely, M., 2014. Dynamic behavior of direct spring loaded pressure relief valves in gas service: model development, measurements and instability mechanisms. J. Loss Prev. Process Ind. 31, 70–81.
Huang, P., Bradshaw, P., Coakley, T., 1993. Skin friction and velocity profile family for compressible turbulent boundary layers. AIAA J. 31 (9).
Jan, C., 1980. Dynamic effects on structures and equipment due to safety relief valve discharge loads. Nucl. Eng. Des. 59, 171–183.
Kasai, K., 1968. On the stability of a poppet valve with an elastic support: 1st report, considering the effect of the inlet piping system. Bull. JSME 11 (48), 1068–1083.
Kim, H.-D., et al., 2006. A study of the gas flow through a LNG safety valve. J. Therm. Sci. 15 (4), 355–360.
Launder, B.E., Spalding, D.B., 1974. The numerical computation of turbulent flows. Comput. Methods Appl. Mech. Eng. 3 (2), 269–289.
Lee, M., Chou, L., Yang, S., 1982. PWR safety/relief valve blowdown analysis experience. Nucl. Eng. Des. 72 (3), 421–427.
Licsko, G., Champneys, A., Hös, C., 2009. Nonlinear analysis of a single stage pressure relief valve. Int. J. Appl. Math 39 (4), 12–26.
MacLeod, G., 1985. Safety valve dynamic instability: an analysis of chatter. J. Press. Vessel Technol. 107 (2), 172–177.
McElhaney, K., 2000. An analysis of check valve performance characteristics based on valve design. Nucl. Eng. Des. 169–182.
Menter, F.R., Kuntz, M., Langtry, R., 2003. Ten years of industrial experience with the SST turbulence model. Turbulence Heat Mass Transfer 4 (1).
Misra, A., Behdinam, K., Cleghorn, W.L., 2002. Self-excited vibration of a controlvalve due to fluid-structure interaction. J. Fluids Struct. 16 (5), 649–665.
Moody, F., 1982. Unsteady piping forces caused by hot water discharge from suddenly opened safety/relief valves. Nucl. Eng. Des. 72 (2), 213–224.
Ono, A., Kimura, N., Kamide, H., Tobita, A., 2011. Influence of elbow curvature on flow structure at elbow outlet under high Reynolds number condition. Nucl. Eng. Des. 241 (11), 4409–4419.
Rolander, N., et al., 2006. An approach to robust design of turbulent convective systems. Am. Soc. Mech. Eng. 128, 844–855.
Sajben, M., Bogar, T., Kroutil, J., 1981. Forced oscillation experiments in supercritical diffuser flows with application to ramjet instabilities. AIAA Paper 1, 487.
Salmon, J., Bogar, T., Sajben, M., 1983. Laser Doppler velocimeter measurements in unsteady, separated, transonic diffuser flows. AIAA J. 21 (12), 1690–1697.
Schmidt, J., Peschel, W., Beune, A., 2009. Experimental and theoretical studies on high pressure safety valves: sizing and design supported by numerical calculations (CFD). Chem. Eng. Technol. 32 (2), 252–262.
Singh, A., 1982. An analytical study of the dynamics and stability of a spring loaded safety valve. Nucl. Eng. Des. 72 (2), 197–204.
Song, X., et al., 2014. A CFD analysis of the dynamics of a direct-operated safety relief valve mounted on a pressure vessel. Energy Convers. Manage. 81, 407–419.
Stern, F., Wilson, R., Coleman, H.W., Paterson, E.G., 2001. Comprehensive approach to verification and validation of CFD simulations—part 1: methodology and procedures. J. Fluids Eng. 123 (4), 793–802.
Sutherland, W., 1893. LII. The viscosity of gases and molecular force. London Edinburgh Dublin Philos. Mag. J. Sci. 36 (223), 507–531.
The American Society of Mechanical Engineers, 2011. ASME BPVC Section I - Rules for Construction of Power Boilers - Certification of Capacity of Pressure Relief Valves - PG-69.2.3. ASME, New York.
Thomann, H., 1976. Oscillations of a simple valve connected to a pipe. Z. Angew. Math. Phys. 27 (1), 23–40.
Vu, B., Wang, T.-S., Shih, M.-H., Soni, B., 1994. Navier-Stokes flow field analysis of compressible flow in a high pressure safety relief valve. Appl. Math. Comput. 65 (1), 345–353.
Wagner, W., 1998. Properties of Water and Steam: The Industrial Standard IAPWS-IF97 for the Thermodynamic Properties and Supplementary Equations for Other Properties: Tables Based on These Equations. Springer Verlag, s.l.
Wilcox, D.C., 1993. Turbulence Modeling for CFD.–Glendale: DCW Industries, first ed. DCW Industries, Inc., California.
Yee, H.C., Klopfer, G.H., Montagne, J.-L., 1990. High-resolution shock-capturing schemes for inviscid and viscous hypersonic flows. J. Comput. Phys. 88 (1), 31–61.
Wilson, R., Stern, F., Coleman, H., Paterson, E., 2001. Comprehensive approach to verification and validation of CFD simulations. 2. Application for RANS simulation of a cargo/container ship. J. Fluids Eng. 123 (4), 803–810.